Supporting Information

Dodge et al. 10.1073/pnas.1308421110

SI Results

Increasing evidence indicates that alterations in energy metabolism play an important role in the pathogenesis of amyotrophic lateral sclerosis (ALS). Metabolic abnormalities in patients with ALS include development of a hypermetabolic phenotype, a gradual loss of body fat that cannot be attributed to decreased energy intake, hyperlipidemia, and a number of hormonal changes (e.g., insulin insensitivity and elevated circulating glucocorticoid and glucagon levels) that affect lipid catabolism (1–6). Similarly, transgenic mice over-expressing the G86R mutation of the Cu/Zn superoxide dismutase 1 (SOD1) gene display lower insulin levels, reduced adipose tissue mass, and an increase in peripheral lipid clearance (7, 8). Consistent with these observations, we recently reported that accelerated disease progression in $SOD1^{G93A}$ mice is positively correlated with circulating levels of the lipolytic hormone, corticosterone (9). Sustained triglyceride catabolism to nonesterified fatty acids followed by β-oxidation to ketone bodies (i.e., acetoacetate, β-hydroxybutyrate, and acetone) has the potential to lead to development of pathological acidosis (10). Interestingly, elevated ketone levels have been reported in both human and mouse models of ALS. For example, in early symptomatic $SOD1^{G86R}$ mice and humans with ALS, serum β-hydroxybutyrate levels are significantly elevated (7, 11). In patients with ALS, levels of acetone in cerebrospinal fluid (CSF) is increased more than twofold (12). Although these metabolic alterations observed during the course of disease appear to favor the development of acidosis, it remains unclear whether this aspect of the disease is pathogenic. Therefore, we determined whether $SOD1^{G93A}$ mice display metabolic changes (i.e., alterations indicative of increased lipolysis) that would favor the development of acidosis.

EchoMRI whole body imaging was used to assess lean and fat mass in male $SOD1^{G93A}$ mice ($n = 12$) following onset and subsequent progression of the disease. Lean and fat mass values in symptomatic (SYMP, abnormal hindlimb splay; median age 75 d) ALS mice were comparable to WT littermate controls (Fig. S3 *A* and *B*). However, end stage (ES, onset of partial paralysis in one limb; median age 103 d) and moribund (MB, unable to right themselves within 30 s after being placed on their back; median age 122 d) ALS mice showed significant ($P < 0.0001$) reductions in both lean and fat mass (Fig. S3 *A* and *B*). It should be noted that ES mice displayed normal food consumption (food was placed on the cage floor starting at symptom onset); therefore, similar to patients with ALS, reductions in mass cannot be attributed to reduced caloric intake.

The breakdown of triglycerides into fatty acids is primarily regulated by lipolytic (e.g., glucagon and corticosterone) and antilipolytic hormones (e.g., insulin) (13). Recently, we reported that higher corticosterone levels in $SOD1^{G93A}$ mice were highly correlated with accelerated paralysis and earlier death (9). Importantly, disease-related changes in serum corticosterone levels were limited to specific circadian time (CT) points, suggesting that ALS mice endure episodes of transient metabolic stress. Here, we determined whether $SOD1^{G93A}$ mice display changes in glucagon and insulin that are consistent with increased lipid metabolism. Trunk blood was collected from male WT, SYMP, and ES mice at CT10 (10:00 AM) and CT18 (6:00 PM) ($n = 8$ per group per time point) for analysis. Measurements were made at CT10 because maximal elevations in corticosterone were noted at this time point in our previous study (9). Additional samples were collected at CT18 because we previously observed no difference in circulating corticosterone levels between WT and $SOD1^{G93A}$ mice at this time point. Similar to what had been reported in $SOD1^{G86R}$ mice (7), the levels of the antilipolytic hormone insulin were significantly ($P < 0.05$) diminished in SYMP and ES $SOD1^{G93A}$ mice vs. WT mice at CT10, but not at CT18 (Fig. S3*D*). Interestingly, as observed in patients with ALS (6), the levels of the lipolytic hormone glucagon were elevated in SYMP and ES mice compared with WT controls at CT10 (Fig. S3*C*). The increase in glucagon was significant ($P < 0.02$) in ES mice. At CT18, no difference in circulating glucagon levels was observed between ALS and WT mice. In agreement with these findings of disease-associated changes in hormonal levels that favor lipolysis, we also recorded a significant decline ($P < 0.01$) in serum triglyceride levels in ES mice at CT10, but not at CT18 (Fig. S3*E*). Similar reductions in serum triglyceride levels have been reported in $SOD1^{G86R}$ mice (8). Collectively, our findings indicate that $SOD1^{G93A}$ mice display several metabolic changes (reduced fat mass, increased corticosterone, elevated glucagon, lower insulin, and decreased triglycerides) that are consistent with the hypothesis that the animals were in a state of heightened lipolysis. These results also highlight the importance of making experimental measurements at various circadian time points to uncover potential underlying neuropathological features in the course of the ALS disease.

SI Materials and Methods

Body Composition and Hormone Measurements. Lean and fat mass in ALS mice (as a function of disease stage) and age-matched WT counterparts were measured with an EchoMRI-100 (EchoMRI) according to the manufacturer's instructions. Measurements were carried out in living, nonsedated mice in less than 1 min. ELISA kits were used to measure serum glucagon (R&D Systems) and insulin (EMD Millipore) levels according to the manufacturer's instructions.

pH Measurements. In vivo pH measurements were made in anesthetized ALS (at different phases of disease) and WT mice (age-matched to ES and MB ALS mice) using a pH Optica system (World Precision Instruments) according to the manufacturer's instructions (14) Briefly, a needle type fiber optic microsensor (with a 140-μm tip size and 0.01-pH resolution) was stereotaxically implanted into various CNS regions [motor cortex, ventral thalamus, lateral ventricle (CSF), brainstem (motor trigeminal nucleus), and lumbar spinal cord] under isoflurane anesthesia. Final measurements were recorded after a 10-min equilibration period (after the sensor was inserted into the targeted region). After the measurements were made, animals were rapidly decapitated (while still anesthetized) to collect trunk blood for pH measurements. Pilot studies (in which pH was measured over a 30-min period) were carried out in WT mice to confirm that isoflurane (0.8%) exposure did not produce measurable changes in pH.

Serum Chemistry Analysis. The VetACE clinical chemistry system (Alpha Wassermann) was used to measure the concentration of analytes (albumin, calcium, and phosphate) in the serum of ALS and WT mice. These spectrophotometric analyses were performed at 37 °C. Sodium, potassium, chloride, and CO_2 levels in serum were determined with a Beckman CX5 clinical chemistry analyzer (Beckman Coulter), which uses indirect ion selective electrode (ISE) methodology to determine the concentration of electrolytes in biological fluids. The Beckman CX5 determines ion concentration by measuring electrolyte activity in solution. When the sample/buffer mixture contacts the electrode, ions

undergo an ion exchange in the hydrated outer layer of the glass electrode, and as the ion exchange takes place, a change in voltage (potential) is developed at the face of the electrode. The potential follows the Nernst equation and allows calculation of electrolyte concentration in a solution.

Glucose and Glycogen Levels. Glucose and glycogen levels in CNS tissue (cerebral cortex, midbrain, cerebellum, brainstem, and lumbar spinal cord) and peripheral tissues (liver, quadriceps muscle, and kidney) were measured as described (15). Briefly, lysates were first digested with α-amyloglucosidase (0.54 mg/mL; Sigma-Aldrich) in 25 mM potassium acetate buffer, pH 5.5. The released glucose in the test samples and the levels of endogenous glucose from undigested samples were quantitated with the Amplex red glucose/glucose oxidase assay kit (Invitrogen). Glycogen levels were determined by subtracting the glucose levels in the undigested samples from those in the digested samples. Bovine liver glycogen (Sigma-Aldrich) was used as a reference standard.

α-Glucosidase Activity Measurements. Tissue α-glucosidase activities were determined using 4-methylumbelliferone-α-D-glucopyranoside as the artificial substrate. Samples were diluted 1:10 in 100 mM sodium acetate containing 0.01% BSA at a pH of 4.3 or 7.0 and then pipetted (15 μL) in duplicate into a 96-well plate. A total of 50 μL of 4-MU-α-D-glucopyranoside substrate was then added to each well and allowed to incubate at 37 °C in the dark for 2 h. The reaction was stopped with glycine-NaOH, pH 12.5 (185 μL per well) and the fluorescence determined with a flourometer at an excitation wavelength of 360 nm and an emission wavelength of 450 nm with a cutoff at 435 nm.

Periodic Acid-Schiff Staining. Tissue sections were deparaffinized, hydrated in water, and oxidized in 0.5% periodic acid solution for 5 min. Sections were then rinsed in distilled water, placed in Schiff reagent for 15 min (during which time the sections become light pink), and then washed in lukewarm tap water for 5 min (sections immediately turn dark pink). Sections were then counterstained with Mayer's hematoxylin for 1 min, washed in tap water for 5 min, dehydrated, and coverslipped with a synthetic mounting medium (Acrytol; Leica Microsystems).

Acetazolamide Administration. Constant release pellets (Innovative Research of America) were implanted in the back of the neck of anesthetized female mice using a trochar (according to the manufacturer's instructions). Acetazolamide (Taro Pharmaceuticals) pellets were designed to deliver 30 mg/kg of drug ($n = 10$) or placebo ($n = 10$) per day over a 90-d period. Groups were sibling matched and mice were implanted with pellets at 60 d of age.

RT-PCR. Cervical spinal cord tissues from B6SJL-Tg(SOD1-G93A) mice were homogenized in Trysol reagent (Sigma-Aldrich) and total RNA was extracted with the miRNeasy Mini kit following the manufacturer's protocol (Qiagen). Total RNA concentration was determined with a NanoDrop 1000 spectrophotometer (ThermoFisher Scientific) by absorbance at 260 nm. cDNA was synthesized with the High-Capacity cDNA Reverse Transcriptase kit (Applied Biosystems), 1.5 μg total RNA serving as template. Gene expression levels were measured by real-time RT-PCR. TaqMan Gene Expression assays (Applied Biosystems) containing specific Mus musculus (Mm) probes and primers [acid sensing ion channel 1 (ASIC1), Mm01305997; ASIC2, Mm00475691; ASIC3, Mm00805460; Mm00448968; Peptidylprolyl Isomerase A (PPIA), Mm02342430] and TaqMan Gene Expression Master mix (Applied Biosystems) were used with 50 ng of cDNA template to determine expression levels of ASIC1, ASIC2, ASIC3, and endogenous control gene Ppia. PCR reactions were performed on the Applied Biosystems 7500 Real-Time PCR system with the following thermal conditions: 50 °C for 2 min, 95 °C for 10 min, and 40 cycles of 95 °C for 15 s, and 60 °C for 1 min. Each reaction was performed in duplicate and in a 96-well format. PCR data were acquired from Sequence Detector Software (SDS version 2.0; Applied Biosystems) and quantified by a standard curve method.

Human Tissue Samples. Human cervical spinal cord segments from nine patients who died of respiratory failure caused by ALS were used (Table S2). Control samples were obtained from seven age-matched individuals without evidence of neurological disease. Human tissue was obtained from the National Institute of Child Health and Human Development Brain and Tissue Bank for Developmental Disorders at the University of Maryland, Baltimore, Contact HHSN275200900011C, Ref. N01-HD-9–0011.

Statistics. Error bars represent ±SEM. Statistical tests were performed either by an analysis of variance (ANOVA) or a two-way ANOVA followed by a Bonferroni post hoc test to find mean differences between groups (GraphPad; Prism software). Survival analysis was conducted by the Kaplan–Meier method. A value of $P < 0.05$ was considered statistically significant.

1. Desport JC, et al. (2001) Factors correlated with hypermetabolism in patients with amyotrophic lateral sclerosis. *Am J Clin Nutr* 74(3):328–334.
2. Dupuis L, et al. (2008) Dyslipidemia is a protective factor in amyotrophic lateral sclerosis. *Neurology* 70(13):1004–1009.
3. Kasarskis EJ, Berryman S, Vanderleest JG, Schneider AR, McClain CJ (1996) Nutritional status of patients with amyotrophic lateral sclerosis: Relation to the proximity of death. *Am J Clin Nutr* 63(1):130–137.
4. Reyes ET, Perurena OH, Festoff BW, Jorgensen R, Moore WV (1984) Insulin resistance in amyotrophic lateral sclerosis. *J Neurol Sci* 63(3):317–324.
5. Patacchioli FR, et al. (2003) Adrenal dysregulation in amyotrophic lateral sclerosis. *J Endocrinol Invest* 26(12):RC23–RC25.
6. Hubbard RW, et al. (1992) Elevated plasma glucagon in amyotrophic lateral sclerosis. *Neurology* 42(8):1532–1534.
7. Dupuis L, Oudart H, René F, Gonzalez de Aguilar JL, Loeffler JP (2004) Evidence for defective energy homeostasis in amyotrophic lateral sclerosis: Benefit of a high-energy diet in a transgenic mouse model. *Proc Natl Acad Sci USA* 101(30):11159–11164.
8. Fergani A, et al. (2007) Increased peripheral lipid clearance in an animal model of amyotrophic lateral sclerosis. *J Lipid Res* 48(7):1571–1580.
9. Fidler JA, et al. (2011) Disease progression in a mouse model of amyotrophic lateral sclerosis: The influence of chronic stress and corticosterone. *FASEB J* 25(12):4369–4377.
10. Sestoft L, Bartels PD (1983) Biochemistry and differential diagnosis of metabolic acidoses. *Clin Endocrinol Metab* 12(2):287–302.
11. Kumar A, et al. (2010) Metabolomic analysis of serum by (1) H NMR spectroscopy in amyotrophic lateral sclerosis. *Clin Chim Acta* 411(7-8):563–567.
12. Blasco H, et al. (2010) 1H-NMR-based metabolomic profiling of CSF in early amyotrophic lateral sclerosis. *PLoS ONE* 5(10):e13223.
13. Jaworski K, Sarkadi-Nagy E, Duncan RE, Ahmadian M, Sul HS (2007) Regulation of triglyceride metabolism. IV. Hormonal regulation of lipolysis in adipose tissue. *Am J Physiol Gastrointest Liver Physiol* 293(1):G1–G4.
14. Friese MA, et al. (2007) Acid-sensing ion channel-1 contributes to axonal degeneration in autoimmune inflammation of the central nervous system. *Nat Med* 13(12):1483–1489.
15. Sidman RL, et al. (2008) Temporal neuropathologic and behavioral phenotype of 6neo/6neo Pompe disease mice. *J Neuropathol Exp Neurol* 67(8):803–818.

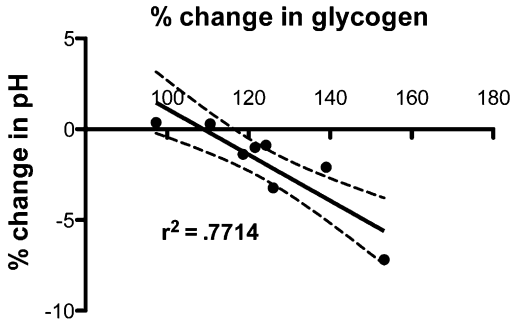

Fig. S1. Glycogen levels correlate with pH in the CNS of ALS mice. The percent reduction in pH (from WT) significantly ($P < 0.004$) correlated ($r^2 = 0.7714$) with the percent increase (from WT) in glycogen accumulation observed within the CNS (cortex, midbrain, brainstem, and lumbar spinal cord) of SYMP and ES ALS mice.

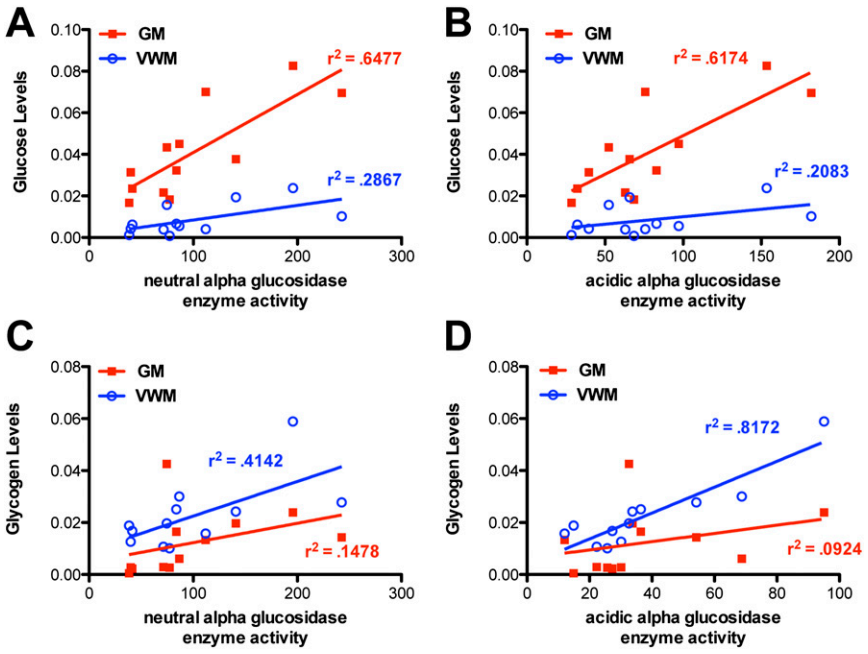

Fig. S2. Glucose and glycogen levels correlate with α-glucosidase enzyme activity in human spinal cord tissue samples. (*A*) Neutral and (*B*) acidic α-glucosidase enzyme activity correlated with glucose levels in gray matter (GM) and ventral white matter (VWM) tissue samples collected from patients with ALS and age-matched controls. Significant ($P < 0.001$) correlations were observed in GM tissue samples for both neutral and acidic enzyme activities. (*C*) Neutral and (*D*) acidic α-glucosidase enzyme activity correlated with glycogen levels in human GM and VWM tissue samples. Significant ($P < 0.001$) correlations were observed in VWM tissue samples for both neutral and acidic enzyme activities.

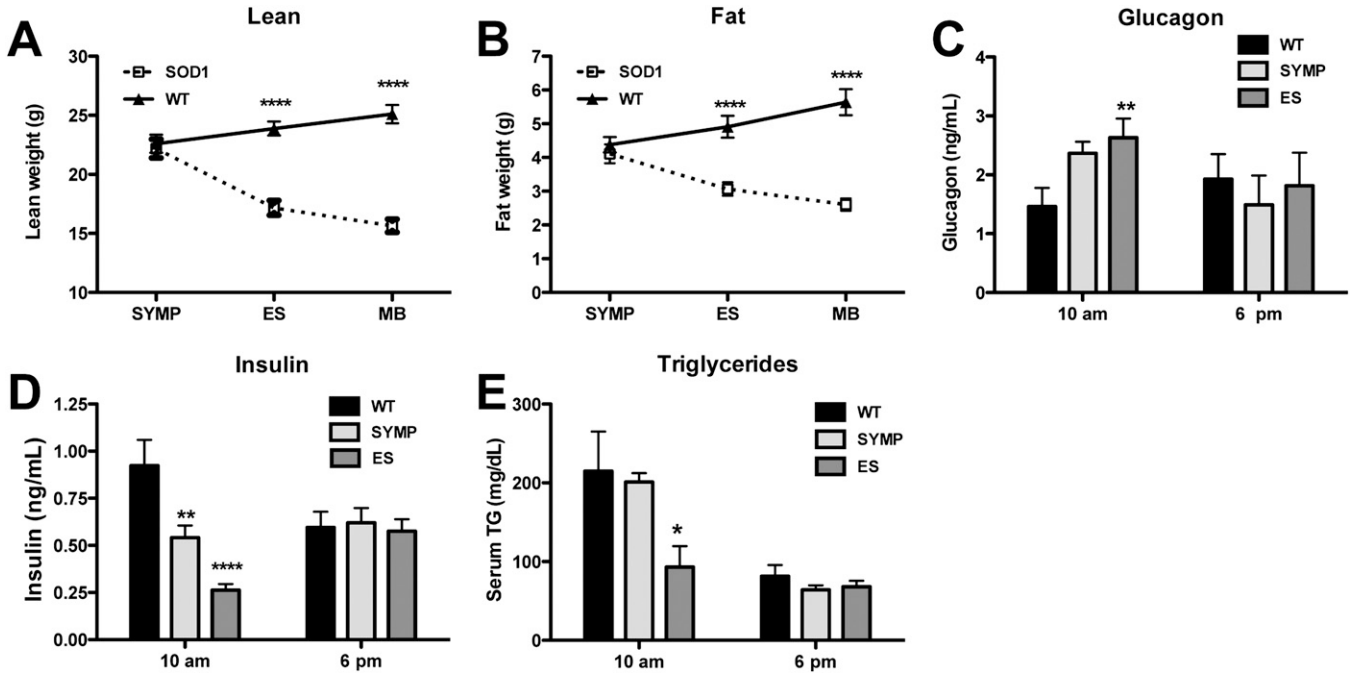

Fig. S3. ALS mice display metabolic alternations (muscle catabolism and increased lipolysis) that favor development of pathological acidosis. (*A*) Lean and (*B*) fat mass composition in ALS mice as a function of disease state vs. WT littermate controls. Serum levels of (*C*) glucagon (lipolytic hormone), (*D*) insulin (antilipolytic hormone), and (*E*) triglyceride were measured in ALS mice as a function of disease state vs. WT littermate controls at different circadian time (CT) points (SYMP, symptomatic, abnormal hindlimb splay, median age 82 d; ES, end stage, onset of limb paralysis (typically hindlimb), median age 103 d; and MB, moribund mouse unable to right itself within 30 s after being place on its back, median age 122 d.) Significantly different from WT (*$P < 0.05$,**$P < 0.02$, ***$P < 0.01$, ****$P < 0.0001$). Error bars represent ±SEM.

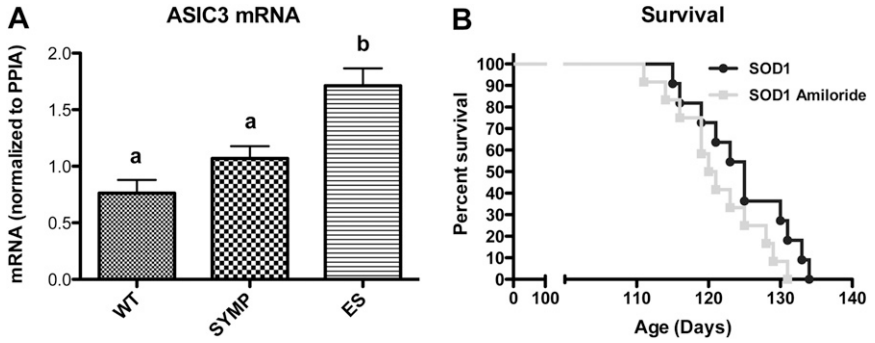

Fig. S4. Acid-sensing ion channel (ASIC) expression in ALS mice and the impact of amiloride treatment on disease progression. (*A*) ASIC3 mRNA (normalized to PPIA) measured in the spinal cords of WT ($n = 8$), SYMP ($n = 8$), and ES ($n = 8$) mice. Bars with different letters are significantly different from each other ($P < 0.01$). Error bars represent ±SEM. (*B*) Survival rates in ALS mice treated with amiloride pellets ($n = 11$) vs. ALS mice treated with placebo/control pellets ($n = 11$). Constant release pellets (Innovative Research of America) were implanted in the back of the neck of anesthetized mice with a trochar (according to the manufacturer's instructions). Amiloride pellets were designed to deliver 10 mg/kg of drug per day over a 90-d period. Mice were implanted with pellets at 60 d of age. No statistical difference in median survival was observed between mice implanted with placebo vs. amiloride pellets (125 d vs. 120 d).

Table S1. Serum concentration of electrolytes that affect H^+ levels

	10:00 AM			6:00 PM		
Electrolyte	WT	SYMP	ES	WT	SYMP	ES
Na^+	140.8 ± 3.59	140.2 ± 2.10	138.8 ± 1.74	136.6 ± 1.73	134.80 ± 1.49	140.6 ± 1.5
K^+	4.00 ± 0.14	3.82 ± 0.13	**3.06 ± 0.43***	3.70 ± 0.02	3.94 ± 0.13	4.10 ± 0.18
Ca^{2+}	4.72 ± 0.02	4.68 ± 0.07	**4.35 ± 0.04***	4.75 ± 0.07	**4.42 ± 0.02**	**4.20 ± 0.03**
Mg^{2+}	2.09 ± 0.07	2.22 ± 0.17	**1.67 ± 0.06***	2.09 ± 0.04	1.97 ± 0.07	1.92 ± 0.08
Cl^-	108.0 ± 2.02	106.2 ± 0.80	105.8 ± 0.80	110.6 ± 1.40	**103.8 ± 1.14***	107.4 ± 1.16
Lactate	6.95 ± 0.44	**4.12 ± 0.24***	**4.33 ± 0.42***	5.89 ± 0.40	**4.90 ± 0.25***	5.80 ± 0.40
CO_2	29.83 ± 2.54	31.8 ± 0.80	32.14 ± 1.96	27.85 ± 2.40	27.91 ± 1.8	32.62 ± 2.26
PO_4^{-3}	2.17 ± 0.15	2.28 ± 0.15	1.94 ± 0.16	1.94 ± 0.87	2.13 ± 0.07	2.05 ± 0.07
Albumin	28.2 ± 0.97	29.8 ± 0.94	26.60 ± 1.96	29.60 ± 2.40	**26.4 ± 0.8***	**26.00 ± 0.36***
SID_{app}	43.02 ± 1.73	44.26 ± 1.65	41.60 ± 1.70	—	—	—
SID_{eff}	46.46 ± 1.85	45.42 ± 1.78	**30.03 ± 1.87***	—	—	—
SIG	−3.44 ± 0.56	−1.16 ± 0.16	11.57 ± 1.22*	—	—	—

Electrolyte concentrations (expressed as mEq/L) were measured in ALS mice as a function of disease state vs. WT littermate controls at different circadian times. ES, end stage; SID_{app}, apparent strong ion difference; SID_{eff}, effective strong ion difference; SIG, strong ion gap; SYMP, symptomatic. Significantly different from WT (*$P < 0.01$). Error bars represent ±SEM.

Table S2. Human tissue donor information

Case no.	Sex	Age at death, y/d	Postmortem interval	Tissue type	Cause of death
1	M	54/40	15	Fixed	ALS
2	M	41/335	21	Fixed	ALS
3	M	59/236	6	Fixed/frozen	ALS
4	M	61/49	8	Fixed/frozen	ALS
5	M	71/17	19	Fixed	ALS
6	M	77/23	3	Fixed/frozen	ALS
7	M	66/245	13	Frozen	ALS
8	M	45/354	19	Frozen	ALS
9	M	88/147	24	Frozen	ALS
10	M	45/364	17	Fixed	Cardiovascular disease
11	M	56/164	22	Frozen	Cardiovascular disease
12	M	59/53	44	Frozen	Pending
13	M	57/305	16	Frozen	Cardiovascular disease
14	M	64/54	13	Frozen	Multiple injuries
15	M	69/296	23	Frozen	Pending
16	M	59/283	18	Frozen	Heroin and alcohol intoxication
17	M	48/242	21	Frozen	Cardiovascular disease